Hyperfine Coupling in Colloidal n-Type ZnO Quantum Dots: Effects on Electron Spin Relaxation

Kelly M. Whitaker, Stefan T. Ochsenbein, Alyssa L. Smith, Dorothy C. Echodu, Bruce H. Robinson, and Daniel R. Gamelin*

Department of Chemistry, University of Washington, Seattle, Washington 98195-1700

Received: July 9, 2010; Revised Manuscript Received: July 26, 2010

Electron spin relaxation dynamics in colloidal ZnO quantum dots containing additional delocalized conduction band electrons (n-type) have been studied using electron paramagnetic resonance (EPR) spectroscopy. Variation of the ^{67}Zn ($I = 5/2$) nuclear isotope content within the quantum dots allows the effects of the electron−nuclear hyperfine interaction on spin−spin and spin−lattice relaxation dynamics to be explored. Long room-temperature spin−spin relaxation times of $T_2 = 87$ ns are observed in ZnO quantum dots almost completely depleted of ^{67}Zn.

Introduction

Colloidal semiconductor nanocrystals are excellent systems for exploring the fundamental properties of quantum-confined charge carriers. Tremendous progress has already been made in understanding the properties of electron−hole pairs (excitons) confined in colloidal quantum dots (QDs) using optical spectroscopic techniques.[1−6] In contrast with charge carriers in QD electronic excited states, the properties of QDs containing excess carriers in their *ground* states have received substantially less attention.[7−19] To date, the primary experimental probe of such charged QDs has been electronic absorption spectroscopy, in which low-energy intraband excitations can be used to define the carrier wave function.

Electron paramagnetic resonance (EPR) spectroscopy is a powerful technique for studying electronic structures and spin relaxation dynamics in various molecular or solid-state species containing unpaired electrons, but this experiment remains almost wholly unexplored for probing charge carriers in colloidal QDs.[15−17,19] For such measurements, colloidal QDs must be prepared that contain additional charge carriers that are stable on the experiment's time scale, and among II−VI semiconductor nanocrystals, to date this technique has been applied only to conduction band electrons in colloidal ZnO quantum dots.[15−17,19] A series of studies of ZnO nanocrystalline powders has also provided important insight into the wave functions of closely related shallow-donor charge carriers.[20−23] Colloidal ZnO nanocrystals possess low-energy conduction band edges, and their rich surface chemistry has allowed the formation of conduction band electrons with extremely long decay constants (on the month time scale),[15] allowing a variety of new experiments to be performed with this motif.[15−17,19]

Here, we present the results of EPR experiments aimed at evaluating electron−nuclear hyperfine interactions in colloidal ZnO QDs. Spin dynamics in ZnO have garnered attention recently, both experimentally[16,24−27] and theoretically.[28,29] ZnO is a particularly interesting semiconductor for studying electron spin relaxation mechanisms because of its low natural nuclear spin content. Of the components of this lattice, only zinc has an isotope with nuclear spin of sizable natural abundance (^{67}Zn, $I = 5/2$, 4.1%).[30] In this study, the nuclear spin contents of colloidal ZnO QDs have been controlled chemically by preparing nanocrystals from precursors containing different concentrations of ^{67}Zn. EPR line shape analysis has allowed the spin−spin and spin−lattice relaxation times to be determined. A significant lengthening of the spin−spin relaxation time is achieved by eliminating ^{67}Zn almost completely, demonstrating the important role electron−nuclear hyperfine coupling plays in QD spin relaxation dynamics.

Experimental Section

A. Nanocrystal Preparation. Colloidal ZnO nanocrystals were synthesized and characterized as described in detail previously.[15,16,31] The ^{67}Zn isotope contents of these nanocrystals were enriched or depleted by changing the concentration of ^{67}Zn in the zinc acetate precursor used in the nanocrystal synthesis step. For preparation of [^{67}Zn] = 0.03% ZnO nanocrystals, the ^{67}Zn-depleted zinc acetate was prepared from ^{67}Zn-depleted zinc metal (EURISO-TOP) that was digested in acetic acid at 60 °C for several days. The resulting zinc acetate was recrystallized and then used as the cation source in the standard nanocrystal preparation. The [^{67}Zn] = 4.1 and 9.6% ZnO QDs were prepared from commercial zinc acetate (Sigma Aldrich and Trace Sciences International) at these isotope levels, and a 50:50 ratio of these two precursors was used to prepare the [^{67}Zn] = 6.9% ZnO nanocrystals. The colloidal ZnO nanocrystal surfaces were capped with either trioctylphosphine oxide (TOPO) or dodecylamine (DDA). Average nanocrystal diameters were determined using established empirical relationships[32] between diameter and band-edge electronic absorption spectra.

B. Photodoping. The colloidal ZnO nanocrystals were dispersed in toluene with a small addition of ethanol (∼1% by volume) and sealed under anaerobic conditions. These nanocrystal suspensions were irradiated with UV light just until an EPR signal could be observed (∼30 s), yielding an average occupancy of $\langle n \rangle \ll 1$ electron per nanocrystal. The EPR intensities described here therefore all come only from nanocrystals containing exactly one unpaired electron. These n-type ZnO nanocrystals are kinetically stable for as long as they remain anaerobic.[15]

C. Electron Paramagnetic Resonance Spectroscopy. CW EPR experiments were performed using X-band Bruker EMX

* To whom correspondence should be addressed. E-mail: gamelin@chem.washington.edu.

10.1021/jp106356y
Published on Web 08/11/2010

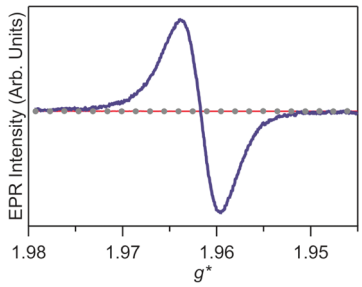

Figure 1. Room-temperature EPR spectra of as-prepared (thin red line), photochemically reduced (thick blue line), and reoxidized (dotted gray line) $d = 7.0 \pm 1.7$ nm colloidal ZnO nanocrystals.

and Bruker E580 spectrometers. Pulsed EPR measurements were performed at 5 K using a Bruker E580 spectrometer with an ER 4118 X-MD5 resonator. Low temperatures were attained with an Oxford Instruments CF935O dynamic continuous flow cryostat with an Oxford Instruments ITC5035 temperature controller, and a Cernox Resistor CX-1050-AA-1.4 L temperature sensor by LakeShore. A $\pi/2-\tau-\pi-\tau$ echo pulse sequence was employed with a 16 ns pulse length for the $\pi/2$ pulse. The decay of the echo intensity I_{echo} was monitored as a function of time delay τ in steps of 4 ns and fit to an exponential of the form $I_{echo} \propto \exp(-2\tau/T_2)$.

D. Linewidth Deconvolution. The CW EPR signals were fit to the derivative of a Lorentzian convolved with a Gaussian using a homemade program in MatLab.[33] A Levenberg−Marquardt routine was used to minimize the square of the difference between the experimental curves and the calculation. Results from this analysis were checked against the Lebedev relation[34] and found to be consistent with it.

Results and Analysis

A. Photodoping. Figure 1 shows the EPR spectra of representative colloidal ZnO QDs collected before photochemical charging, after photochemical charging, and following reoxidation of the n-type QDs upon exposure to air. Prior to charging, there is no detectable EPR signal. Upon photochemical reduction, an EPR signal appears at $g^* \sim 1.96$ that has been attributed to the delocalized conduction band electron.[15−17] The dependence of the electron g^* value on ZnO QD diameter has been described elsewhere.[17] As shown previously,[15−17] this EPR signal intensity correlates with a bleaching of the first excitonic transition and appearance of a new absorption band in the infrared, and all of these spectral changes are reversed upon exposure of the QDs to air.

B. Spin−Spin Relaxation Time, T_2. The EPR signal in Figure 1 has a Voigtian line shape. The width of this EPR line is inversely proportional to the ensemble spin dephasing time constant T_2^*, as described by eq 1a, where Γ_T is the total peak-to-peak EPR line width and γ_e is the electron gyromagnetic ratio. Using eq 1a, a value of $T_2^* = 15$ ns is estimated from the spectrum in Figure 1. This T_2^* value is comparable to that measured on similar colloidal ZnO QDs by time-resolved Faraday rotation (TRFR) spectroscopy at 10 K ($T_2^* > \sim 1.0$ ns).[26] Intuitively, one might have expected that T_2^* would be greater at 10 K than at room temperature. We therefore note that TRFR spectroscopy measures T_2^* following photoexcitation, and electron−hole interactions in the photoexcited state may accelerate spin dephasing. In the present EPR experiments, the hole is removed and the measured T_2^* is that of the electron alone in its ground electronic state.

$$T_2^* = \frac{2}{\gamma_e \Gamma_T} \tag{1a}$$

$$T_2 = \frac{2}{\gamma_e \Gamma_L} \tag{1b}$$

Some of this EPR line width may come from inhomogeneous broadening associated with the size distribution of the ZnO QD ensemble due to the size dependence of g^*,[17] and some comes from unresolved hyperfine splittings (*vide infra*). To extract the homogeneous component, the EPR spectrum was fit with the first derivative of a Lorentzian function convolved with a Gaussian function. This analysis allows separation of the Lorentzian (Γ_L, homogeneous) and Gaussian (Γ_G, inhomogeneous) contributions to the overall line width.[33] From Γ_L, the average homogeneous spin−spin relaxation time, T_2, can be determined using eq 1b, independent of the distribution in resonance frequencies that contribute to T_2^*. For example, by this approach, the data in Figure 1 yield $\Gamma_L = 2.3$ G, and hence $T_2 = 48.6$ ns.

CW-EPR spectra of a series of ZnO QD samples with various ^{67}Zn nuclear spin concentrations ([^{67}Zn]) were collected at room temperature, and the above line shape analysis was performed. Figure 2A shows representative EPR spectra of n-type ZnO QDs with [^{67}Zn] = 0.03 and 9.6%. Substantial broadening and a small shift of the resonance position are apparent for the sample with larger [^{67}Zn]. The shift is due to the slightly different sizes of the two samples ($d = 3.2$ nm for the [^{67}Zn] = 0.03% QDs, $d = 4.0$ nm for the [^{67}Zn] = 9.6% QDs).[17] Lineshape analysis shows that the broadening is mostly due to a greater homogeneous line width (Γ_L) in the nanocrystals with [^{67}Zn] = 9.6%. The line broadening with increasing [^{67}Zn] seen in Figure 2A by visual inspection thus directly reveals the increasing spin−spin relaxation rate with increasing [^{67}Zn]. More quantitatively, line width deconvolution of the spectra in Figure 2A yields the room-temperature time constants $T_2 = 87$ ns for [^{67}Zn] = 0.03% and $T_2 = 24$ ns for [^{67}Zn] = 9.6%. These data are plotted in Figure 2B along with data for QDs of other nuclear spin concentrations, revealing a strong dependence of T_2 on [^{67}Zn]. The inset to Figure 2B plots the same data as $1/T_2$ vs [^{67}Zn], yielding an approximately linear relationship. A linear dependence of the spin−spin relaxation rate due to fluctuations of the nuclear field is expected from theory.[35,36] In contrast to the theoretical prediction, however, a constant offset had to be introduced to fit the data, suggesting an additional relaxation process independent of [^{67}Zn]. This latter process could potentially involve nuclear spins of surface capping ligands, like ^{1}H, ^{31}P (in TOPO), ^{15}N (in DDA), or possibly even solvent molecules.

As an independent check of the T_2 values obtained from the line shape analysis presented above, pulsed EPR experiments were performed on some of the same QDs at low temperatures, and T_2 was determined from the spin echo decay kinetics. Figure 3 shows an echo decay curve measured at 5 K for a $d = 4.0$ nm, [^{67}Zn] = 4.1% QD sample. Fitting these data to a single-exponential decay function yields $T_2 = 79$ ns, which is comparable to the T_2 value of ~55 ns estimated from analysis of the 6 K CW EPR line shape observed for the same sample (Figure 3, inset), lending credence to the results obtained from the line shape analysis. The line shape analysis has the advantage that it can be performed at all temperatures, whereas spin−echoes were only observed at low temperatures.

C. Spin−Lattice Relaxation Time, T_1. The spin−lattice relaxation times (T_1) of these colloidal n-type ZnO QDs were

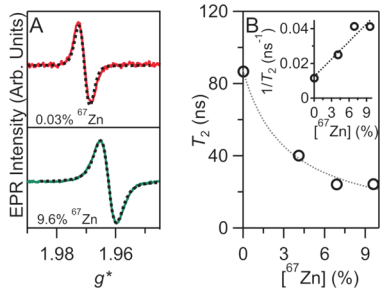

Figure 2. (A) Room-temperature EPR spectra of colloidal n-type ZnO nanocrystals with [^{67}Zn] = 0.03% (top) and [^{67}Zn] = 9.6% (bottom). The dotted lines are the Voigtian fits as described in the text, yielding Γ_L = 1.4 G and Γ_G = 6.6 G for the [^{67}Zn] = 0.03% nanocrystals and Γ_L = 4.7 G and Γ_G = 7.2 G for the [^{67}Zn] = 9.6% nanocrystals. (B) Plot of T_2 as a function of [^{67}Zn], measured at room temperature. Inset: $1/T_2$ plotted vs [^{67}Zn], measured at room temperature. Diameters: d = 3.2 nm for the [^{67}Zn] = 0.03% nanocrystals and d = 4.0 nm for the [^{67}Zn] = 4.1, 6.9, and 9.6% nanocrystals.

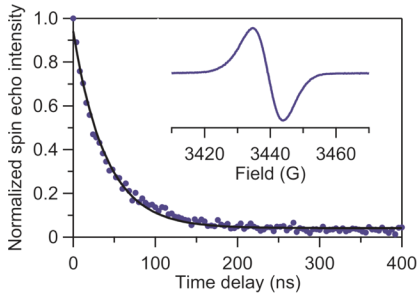

Figure 3. Spin−echo decay curve measured for a frozen suspension of colloidal n-type ZnO nanocrystals (d = 4.0 nm, [^{67}Zn] = 4.1%) at 5 K. The inset shows the corresponding 6 K CW EPR spectrum.

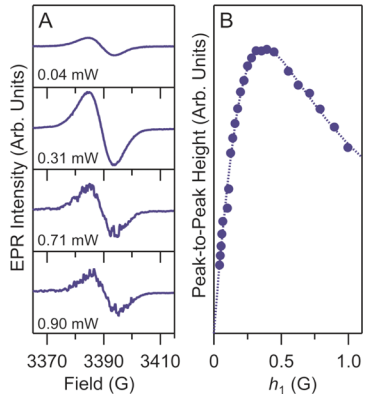

Figure 4. (A) Representative 80 K CW-EPR spectra of colloidal n-type ZnO nanocrystals (d = 4.0 nm, [^{67}Zn] = 4.1%) collected at various microwave powers, $(h_1)^2$. (B) Peak-to-peak heights (ΔY) of the EPR signal plotted as a function of amplitude h_1. The dotted line in part B is a fit to eq 2a yielding P_2 = 0.14 G^2 and ε = 0.96. From the line width analysis, T_2 = 55 ns, and hence, T_1 = 0.8 μs is deduced from eq 2b.

also examined as a function of temperature and nuclear spin concentration. T_1 values were obtained from analysis of EPR power saturation rollover data.[37] In this experiment, a series of EPR spectra are collected at various applied powers traversing from the low-power limit to saturation conditions, and changes in their lineshapes are analyzed to yield relaxation dynamics. Representative spectra at various powers are shown in Figure 4A for a d = 4.0 nm, [^{67}Zn] = 4.1% QD sample, measured at 80 K. Figure 4B plots the peak-to-peak height (ΔY) vs the microwave amplitude (h_1). For small amplitudes, ΔY increases approximately linearly with increasing h_1, but at elevated

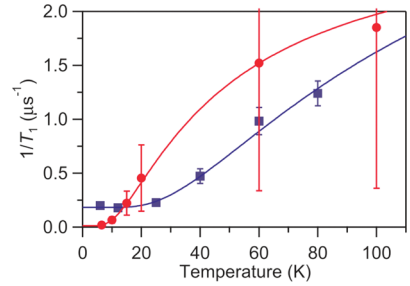

Figure 5. Temperature dependence of $1/T_1$ for d = 4.5 nm, [^{67}Zn] = 0.03% n-type ZnO nanocrystals (●) and d = 4.0 nm, [^{67}Zn] = 4.1% n-type ZnO nanocrystals (■), obtained from analysis of power saturation rollover data as described in the text. The solid lines are fits to eq 3 yielding the parameter values c_0 = 0.01 ± 0.01 μs^{-1} and ΔE = 3.4 ± 0.9 meV for the [^{67}Zn] = 0.03% ZnO nanocrystals and c_0 = 0.18 ± 0.02 μs^{-1} and ΔE = 9.2 ± 1.4 meV for the [^{67}Zn] = 4.1% ZnO nanocrystals.

amplitudes, it rolls over and begins to decrease with increasing h_1. This behavior reflects changes in the EPR line shape as the saturation conditions are reached, and hence contains information about relaxation dynamics. Quantitatively, the saturation rollover data can be described using eq 2a,[37] where P_2 is proportional to the product of the spin−spin ($R_2 = 1/T_2$) and spin−lattice ($R_1 = 1/T_1$) relaxation rates, ε is a measure of the homogeneity of the line width, and c is a scaling constant. Because T_2 is known from the EPR line width analysis, T_1 can be obtained from P_2 using eq 2b. From the data in Figure 4, eqs 2a and 2b yield T_1 = 0.8 μs at 80 K.

$$\Delta Y = c\frac{h_1}{\left(1 + \frac{(h_1)^2}{P_2}\right)^{\varepsilon}} \tag{2a}$$

$$P_2 = \frac{1}{\gamma_e^2}(R_1 \cdot R_2) = \frac{1}{\gamma_e^2}\left(\frac{1}{T_1} \cdot \frac{1}{T_2}\right) \tag{2b}$$

To explore the mechanisms that determine T_1 in these n-type ZnO QDs, power saturation rollover data were collected as a function of temperature for various samples. Figure 5 shows representative data collected for [^{67}Zn] = 0.03% ZnO QDs (d = 4.5 nm) and [^{67}Zn] = 4.1% ZnO QDs (d = 4.0 nm), plotted as $1/T_1$ vs temperature. At the lowest temperatures, $1/T_1$ of the [^{67}Zn] = 0.03% ZnO QDs approaches zero, reaching a value of ~0.019 μs^{-1} at 6.5 K, which corresponds to a T_1 of 54 μs. $1/T_1$ of the [^{67}Zn] = 4.1% ZnO QDs, on the other hand, plateaus at $1/T_1$ = 0.20 μs^{-1} at 6 K (T_1 = 5 μs). The primary intrinsic difference between the two samples is the concentration of nuclear spins (there is also a small size difference of 0.5 nm in diameter), suggesting that if this difference in T_1 were intrinsic then a nuclear-spin-dependent effect would have to dominate the spin−lattice relaxation even at low temperatures. In principle, phonon-modulated hyperfine interactions could contribute to the spin−lattice relaxation,[38] but from the theory derived for phonon-modulated hyperfine interactions in epitaxial QDs,[39] this contribution is expected to be negligible at the lowest temperatures, where no phonons are thermally excited. The observation of a temperature-independent but nuclear-spin-dependent contribution to $1/T_1$ is therefore unexpected and cannot be readily explained solely on the basis of intrinsic effects. An alternative possibility that is difficult to rule out involves differences in adventitious impurities in the Zn

precursors used to prepare the QDs, one being commercial $Zn(OAc)_2$ and the other being isotopically depleted Zn metal.[40]

Despite this difference at low temperature, the behavior of $1/T_1$ with increasing temperature is fairly similar for the two nuclear spin concentrations, and both data sets can be fit to the exponential described by eq 3, which describes thermally activated spin−lattice relaxation. In eq 3, ΔE represents the activation energy, k is the Boltzmann constant, T is the temperature, A is a scaling factor, and c_0 represents the low-temperature limit discussed above. The exponential increase with temperature observed in both data sets in Figure 5 is consistent with an Orbach mechanism. In the [^{67}Zn] = 4.1% ZnO QDs, additional phonon-modulated hyperfine interactions are also possible but evidently not dominant, because these would lead to faster relaxation rates at all temperatures for the sample with the higher nuclear spin concentration. The ΔE values determined for the two samples are somewhat different, at 3.4 ± 0.9 meV for the [^{67}Zn] = 0.03% ZnO QDs and 9.2 ± 1.4 meV for the [^{67}Zn] = 4.1% ZnO QDs. They are, however, on the same order of magnitude, and their difference may simply reflect the increasing difficulty of measuring reliable saturation rollover data at higher temperatures for the [^{67}Zn] = 0.03% ZnO QDs, as indicated by the error bars of Figure 5. The lowest energy optical phonon mode in ZnO that might contribute to T_1 occurs at 12.5 meV,[41] on the same order of magnitude as the experimental ΔE values, supporting interpretation of the data in Figure 5 as reflecting an Orbach process. Additionally, it has been shown that ligand vibrations contribute to intraband carrier relaxation in colloidal CdSe QDs,[42] and an analogous coupling likely also contributes to the spin−lattice relaxation in these n-type QDs.

$$\frac{1}{T_1} = c_0 + A\exp(-\Delta E/kT) \tag{3}$$

Finally, in the limit where interactions between the electron and all nuclear spins (and other electron spins) are completely eliminated, $1/T_2$ should approach $1/(2T_1)$. This limit has been approached in some cases, e.g., for the phosphorus shallow donor defect in isotopically purified Si crystals, where above ~10 K the spin−lattice relaxation is the governing factor for spin relaxation,[43] but the n-type ZnO QDs investigated here are far from this limit in all cases. Even in [^{67}Zn] = 0.03% ZnO QDs, which contain virtually no nuclear spins within the QDs, a sizable difference between $1/(2T_1) = 0.76\ \mu s^{-1}$ and $1/T_2 = 37\ \mu s^{-1}$ at 60 K is observed. This result implicates coupling of the conduction band electrons with other unidentified nuclear spins, the most likely candidates again being those found in the surface capping ligands. Other sources of accelerated spin−spin relaxation could be paramagnetic impurities that are silent in our EPR experiments, or interactions between electron spins of different QDs. Concentration experiments shown no indication of the latter, and given the dilute colloidal nature of the QD samples used here along with the low average electron concentrations ($\langle n\rangle \ll 1$), this possibility can safely be neglected.

D. Inhomogeneous Broadening. As described in section A, the observed EPR signal can be deconvolved into a Lorentzian (homogeneous) contribution, whose width Γ_L is determined by the spin−spin relaxation time T_2, and a Gaussian (inhomogeneous) part Γ_G, which reflects broadening due to the QD size distribution and the distribution of unresolved hyperfine splitting from interactions with the ^{67}Zn nuclei. The size of the hyperfine splitting is determined by the average electron density at the ^{67}Zn nuclei in the QDs, and is therefore governed by the sizes of the QDs and the concentrations of ^{67}Zn within them. For the same [^{67}Zn], reducing the QD diameter results in greater overlap of the electron wave function with the ^{67}Zn nuclei, and thus a stronger average hyperfine interaction with fewer ^{67}Zn nuclei. Equation 4 describes this relationship quantitatively as the Gaussian line width arising from nuclear spin fluctuations for the average ZnO particle.[34,44]

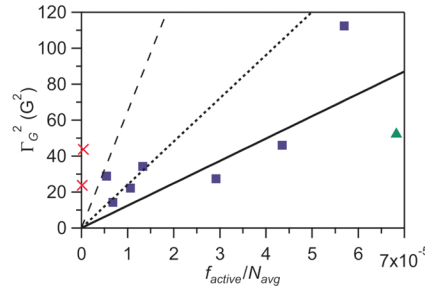

Figure 6. Square of the room-temperature Gaussian EPR line width (Γ_G) vs f_{active}/N_{avg} for [^{67}Zn] = 4.1% (various diameters, 3.2 nm ≤ d ≤ 7 nm) (■), [^{67}Zn] = 0.03% (d = 4.5 and 3.2 nm) (×), and [^{67}Zn] = 9.6% (d = 4.0 nm) (▲) n-type ZnO nanocrystals. The solid line is a linear best fit with the intercept fixed at 0 G^2, yielding a slope of 1.2 × 10^6 G^2. From eq 4, this line corresponds to a_1 = 321 G (3.7 μeV). The dotted and dashed lines are the behaviors expected from the literature theoretical values a_1 = 454 G (5.26 μeV)[45] and 746 G (8.64 μeV)[46] for isolated Zn^+, calculated using eq 4.

$$\Gamma_G = \left[\frac{4}{3}[I(I+1)]\left(\frac{f_{active}a_1^2}{N_{avg}}\right)\right]^{1/2} \tag{4}$$

In eq 4, f_{active} = [^{67}Zn]/100% represents the fraction of spin-active nuclei, N_{avg} is the average total number of cations per QD, I is the relevant nuclear spin quantum number (I = 5/2 for ^{67}Zn), and a_1 is the intrinsic contact hyperfine interaction strength, i.e., the electron−nuclear coupling strength that would result if all of the unpaired electron density were associated with a single $^{67}Zn^+$ ion in the ZnO lattice.

From eq 4, the square of the Gaussian line width should depend linearly on the ratio f_{active}/N_{avg} if other factors such as nanocrystal size distributions can be neglected. The slope of this linear dependence would then be proportional to a_1^2. Figure 6 plots Γ_G^2 vs f_{active}/N_{avg} for the entire set of [^{67}Zn] = 0.03, 4.1, and 9.6% ZnO QDs. Overall, the data are suggestive of a small increase in Gaussian line width with increasing [^{67}Zn], but quantitative analysis is hampered by the scatter in the data set, attributed to inhomogeneous size effects. Despite this scatter, the data do appear to show a ^{67}Zn hyperfine coupling constant that is substantially smaller than existing literature estimates for a_1 of atomic ^{67}Zn. For example, if the data are analyzed according to eq 4 despite the scatter, a_1 = 320 ± 130 G (3.7 ± 1.5 μeV) is estimated when the intercept is fixed at the origin. Even smaller values of a_1 are obtained when the intercept is allowed to be nonzero (best-fit a_1 = 260 G (3.0 μeV)). This experimental a_1 is substantially smaller than the theoretical values of a_1 = 454 G (5.26 μeV) and a_1 = 746 G (8.64 μeV) calculated for unit spin density in the 4s orbital of a $^{67}Zn^+$ ion using Hartree−Fock[45] and Hermann−Skillmann[46] wave functions, respectively. To illustrate, lines calculated from eq 4 using these values are included in Figure 6, where they are seen to be inconsistent with the complete experimental data set.

The reduced value of a_1 obtained from experiment is interpreted as reflecting the important role covalency plays in diminishing contact hyperfine coupling strengths. For example,

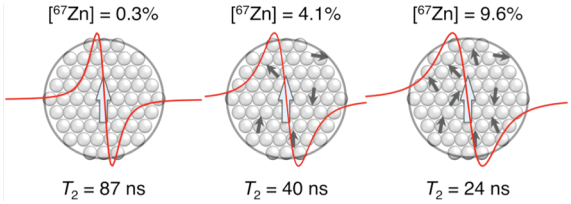

Figure 7. Schematic representation of the dependence of T_2 on nuclear spin content of colloidal n-type ZnO nanocrystals, as reflected in the CW EPR line width. As the nuclear spin content decreases from [^{67}Zn] = 9.6 to 0.03%, the room-temperature T_2 increases by a factor of ~3.5 and the EPR resonance narrows.

DFT calculations estimate ~10% oxygen 2p character in the ZnO conduction band-edge wave function,[47] which delocalizes the electron spin density away from the ^{67}Zn nucleus relative to the electron isolated on Zn^+ that was considered theoretically.[45,46] Furthermore, the sizable difference between the two computed values implies rather large uncertainties even in theoretical estimates, and places greater importance on experimental determination of this hyperfine interaction strength.

Conclusions

The spin dynamics of quantum confined charge carriers in colloidal semiconductor nanocrystals have been explored experimentally using conventional EPR techniques. The nuclear spin content of these nanocrystals was varied by synthesis from precursors with different concentrations of the only abundant spin-active nucleus, ^{67}Zn. The experiments described here demonstrate that these ^{67}Zn nuclear spins dominate the spin−spin relaxation dynamics of conduction band electrons in colloidal ZnO QDs. The effect of changing the nuclear spin content on the spin−spin relaxation time is summarized schematically in Figure 7. A relatively long room-temperature value of $T_2 = 87$ ns was measured in [^{67}Zn] = 0.03% ZnO QDs, which is over 2 times longer than that of comparable natural-abundance ZnO QDs ([^{67}Zn] = 4.1%, $T_2 = 40$ ns) and over 3 times longer than that of ^{67}Zn-enriched ZnO QDs ([^{67}Zn] = 9.6%, $T_2 = 24$ ns). With these data, it was possible to estimate the hyperfine contact term a_1 for ^{67}Zn experimentally for the first time. The same nanocrystals displayed microsecond spin−lattice relaxation times at cryogenic temperatures, with T_1 temperature dependence suggestive of dominant Orbach processes at higher temperatures.

The results presented here are related to those obtained from studies of nitrogen-vacancy centers in diamond (NV^-) and phosphorus donors in silicon (Si:P). In both cases, elongated spin−spin relaxation times were observed after reducing the concentration of spin-active nuclei in the host lattice. An extremely long room-temperature T_2 value of 1.8 ms was found for the NV^- center in ^{13}C-depleted diamond.[48] The NV^- center is a very localized defect, however, and its electron density is distributed over only approximately four atoms.[49] The confined conduction-band electrons described here are therefore perhaps more closely related to the electrons of the phosphorus shallow donor in silicon (Si:P), which is estimated to have an effective Bohr radius of 1.73 nm,[50] comparable to the radii of the QDs studied here. In ^{29}Si-depleted Si:P, T_2 reaches 500 μs at 1.4 K, while T_1 seems independent of nuclear spin concentration ($T_1 \approx 50$ s at 1.4 K).[43,51] The values for T_2 and T_1 for the ^{67}Zn-depleted n-type ZnO QDs studied here are substantially shorter than those of both NV^- and Si:P, which points to an important role played by surface ligands. These data furthermore raise the possibility that extrinsic contributions to relaxation derived from coupling of conduction-band electrons with nuclear spins of the QD surface-capping ligands could be studied by EPR spectroscopy once all or most of the intrinsic ^{67}Zn contributions are suppressed. Future studies of this weak carrier−ligand interaction may provide interesting quantitative insights into this interaction complementary to the recent observation that dipolar coupling with surface ligand vibrations can mediate intra-conduction-band electron relaxation dynamics.[42] Finally, an additional important aspect of the confined electron spins studied here is that they can be gated, providing the ability to control QD physical properties via external perturbations, such as in the recently reported charge-state-controlled magnetism of colloidal Mn^{2+}-doped ZnO QDs.[19] This feature, combined with the preparation of these ZnO QDs as colloids, may ultimately allow the development of gated spin-based device structures using simple and inexpensive solution processing techniques.

Acknowledgment. This work was funded by the NSF ((CRC-0628252) to D.R.G. and DGE-0504573 (IGERT fellowship) to K.M.W.) and the Sloan Foundation. Instrumentation support from NIH (high-end instrumentation) Grant No. S10 RR023065 and from the Center for Ecogenetics and Environmental Health (UW NIH center Grant No. P30 ES07033) is gratefully acknowledged. Robert Nielsen is acknowledged for helpful discussions.

References and Notes

(1) Alivisatos, A. P. Semiconductor Clusters, Nanocrystals and Quantum Dots. *Science* **1996**, *271*, 933–937.
(2) Nirmal, M.; Brus, L. Luminescence Photophysics in Semiconductor Nanocrystals. *Acc. Chem. Res.* **1999**, *32*, 407–414.
(3) Efros, A. L. Fine Structure and Polarization Properties of Band-Edge Excitons in Semiconductor Nanocrystals. In *Semiconductor and Metal Nanocrystals*; Klimov, V. I., Ed.; Marcel Dekker, Inc.: New York, 2004; Vol. 1, pp 103−141.
(4) Klimov, V. I. Mechanism for Photogeneration and Recombination of Multiexcitons in Semiconductor Nanocrystals: Implications for Lasing and Solar Energy Conversion. *J. Phys. Chem. B* **2006**, *110*, 16827–16845.
(5) Scholes, G. D. Controlling the Optical Properties of Inorganic Nanoparticles. *Adv. Funct. Mater.* **2008**, *18*, 1157–1172.
(6) Kim, J.; Wong, C. Y.; Scholes, G. D. Exciton Fine Structure and Spin Relaxation in Semiconductor Colloidal Quantum Dots. *Acc. Chem. Res.* **2009**, *42*, 1037–1046.
(7) Haase, M.; Weller, H.; Henglein, A. Photochemistry and Radiation Chemistry of Colloidal Semiconductors. 23. Electron Storage on ZnO Particles and Size Quantization. *J. Phys. Chem.* **1988**, *92*, 482–487.
(8) Hoyer, P.; Weller, H. Size-dependent redox potentials of quantized zinc oxide measured with an optically transparent thin layer electrode. *Chem. Phys. Lett.* **1994**, *221*, 379–384.
(9) Shim, M.; Guyot-Sionnest, P. n-type colloidal semiconductor nanocrystals. *Nature* **2000**, *407*, 981–983.
(10) Roest, A. L.; Kelly, J. J.; Vanmaekelbergh, D.; Meulenkamp, E. A. Staircase in the Electron Mobility of a ZnO Quantum Dot Assembly due to Shell Filling. *Phys. Rev. Lett.* **2002**, *89*, 036801.
(11) Shim, M.; Wang, C.; Guyot-Sionnest, P. Charge-Tunable Optical Properties in Colloidal Semiconductor Nanocrystals. *J. Phys. Chem. B* **2001**, *105*, 2369–2373.
(12) Shim, M.; Guyot-Sionnest, P. Organic-Capped ZnO Nanocrystals: Synthesis and n-Type Character. *J. Am. Chem. Soc.* **2001**, *123*, 11651–11654.
(13) Germeau, A.; Roest, A. L.; Vanmaekelbergh, D.; Allan, G.; Delerue, C.; Meulenkamp, E. A. Optical Transitions in Artificial Few-Electron Atoms Strongly Confined inside ZnO Nanocrystals. *Phys. Rev. Lett.* **2003**, *90*, 097401.
(14) Shim, M.; Guyot-Sionnest, P. Comment on "Staircase in the Electron Mobility of a ZnO Quantum Dot Assembly due to Shell Filling" and "Optical Transitions in Artificial Few-Electron Atoms Strongly Confined inside ZnO Nanocrystals. *Phys. Rev. Lett.* **2003**, *91*, 169703.
(15) Liu, W. K.; Whitaker, K. M.; Kittilstved, K. R.; Gamelin, D. R. Stable Photogenerated Carriers in Magnetic Semiconductor Nanocrystals. *J. Am. Chem. Soc.* **2006**, *128*, 3910–3911.
(16) Liu, W. K.; Whitaker, K. M.; Smith, A. L.; Kittilstved, K. R.; Robinson, B. H.; Gamelin, D. R. Room-Temperature Electron Spin Dynamics in Free-Standing ZnO Quantum Dots. *Phys. Rev. Lett.* **2007**, *98*, 186804.

(17) Whitaker, K. M.; Ochsenbein, S. T.; Polinger, V. Z.; Gamelin, D. R. Electron Confinement Effects in the EPR Spectra of Colloidal n-type ZnO Quantum Dots. *J. Phys. Chem. C* **2008**, *112*, 14331–14335.

(18) Guyot-Sionnest, P. Charging colloidal quantum dots by electrochemistry. *Microchim. Acta* **2008**, *160*, 309–314.

(19) Ochsenbein, S. T.; Feng, Y.; Whitaker, K. M.; Badaeva, E.; Liu, W. K.; Li, X.; Gamelin, D. R. Charge-Controlled Magnetism in Colloidal Doped Semiconductor Nanocrystals. *Nat. Nanotechnol.* **2009**, *4*, 681–687.

(20) Zhou, H.; Hofstaetter, A.; Hofmann, D. M.; Meyer, B. K. Magnetic resonance studies on ZnO nanocrystals. *Microelectron. Eng.* **2003**, *66*, 59–64.

(21) Orlinskii, S. B.; Schmidt, J.; Baranov, P. G.; Hofmann, D. M.; de Mello Donega, C.; Meijerink, A. Probing the wave function of shallow Li and Na donors in ZnO nanoparticles. *Phys. Rev. Lett.* **2004**, *92*, 047603.

(22) Orlinskii, S. B.; Schmidt, J.; Groenen, E. J. J.; Baranov, P. G.; de Mello Donega, C.; Meijerink, A. Shallow Donors in Semiconductor Nanoparticles: Limit on the Effective Mass Approximation. *Phys. Rev. Lett.* **2005**, *94*, 097602.

(23) Orlinskii, S. B.; Blok, H.; Schmidt, J.; Baranov, P. G.; de Mello Donegá, C.; Meijerink, A. Donor-acceptor pairs in the confined structure of ZnO nanocrystals. *Phys. Rev. B* **2006**, *74*, 045204.

(24) Ghosh, S.; Sih, V.; Lau, W. H.; Awschalom, D. D.; Bae, S.-Y.; Wang, S.; Vaidya, S.; Chapline, G. Room-temperature spin coherence in ZnO. *Appl. Phys. Lett.* **2005**, *86*, 232507.

(25) Ghosh, S.; Steuerman, D. W.; Maertz, B.; Ohtani, K.; Xu, H.; Ohno, H.; Awschalom, D. D. Electrical control of spin coherence in ZnO. *Appl. Phys. Lett.* **2008**, *92*, 162109.

(26) Janssen, N.; Whitaker, K. M.; Gamelin, D. R.; Bratschitsch, R. Ultrafast Spin Dynamcis in Colloidal ZnO Quantum Dots. *Nano Lett.* **2008**, *8*, 1991–1994.

(27) Buyanova, I. A.; Murayama, A.; Furuta, T.; Oka, Y.; Norton, D. P.; Pearton, S. J.; Osinsky, A.; Dong, J. W.; Tu, C. W.; Chen, W. M. Spin Dynamics in ZnO-Based Materials. *J. Supercond. Novel Magn.* **2010**, *23*, 161–165.

(28) Harmon, N. J.; Putikka, W. O.; Joynt, R. Theory of electron spin relaxation in ZnO. *Phys. Rev. B* **2009**, *79*, 115204.

(29) Tribollet, J. Theory of the electron and nuclear spin coherence times of shallow donor spin qubits in isotopically and chemically purified zinc oxide. *Eur. Phys. J. B* **2009**, *72*, 531–540.

(30) Holden, N. E. Table of the Isotopes. In *CRC Handbook of Chemistry and Physics*, 86th ed.; CRC Press: Boca Raton, FL, 2005.

(31) Schwartz, D. A.; Norberg, N. S.; Nguyen, Q. P.; Parker, J. M.; Gamelin, D. R. Magnetic Quantum Dots: Synthesis, Spectroscopy, and Magnetism of Co^{2+}- and Ni^{2+}-Doped ZnO Nanocrystals. *J. Am. Chem. Soc.* **2003**, *125*, 13205–13218.

(32) Meulenkamp, E. A. Synthesis and Growth of ZnO Nanoparticles. *J. Phys. Chem. B* **1998**, *102*, 5566–5572.

(33) Smirnov, A. I.; Belford, R. L. Rapid quantitation from inhomogeneously broadened EPR spectra by a fast convolution algorithm. *J. Magn. Reson., Ser. A* **1995**, *113*, 65–73.

(34) Bales, B. L. Inhomogeneously Broadened Spin-Label Spectra. In *Spin Laveling: Theory and Applications*; Berliner, L. J., Ed.; Academic Press: New York, 1975.

(35) Semenov, Y. G.; Kim, K. W. Phonon-Mediated Electron-Spin Phase Diffusion in a Quantum Dot. *Phys. Rev. Lett.* **2004**, *92*, 026601.

(36) Semenov, Y. G.; Kim, K. W. Elastic spin-relaxation processes in semiconductor quantum dots. *Phys. Rev. B* **2007**, *75*, 195342.

(37) Lin, Y.; Nielsen, R.; Murray, D.; Hubbell, W. L.; Mailer, C.; Robinson, B. H.; Gelb, M. H. Docking Phospholipase A2 on Membranes Using Electrostatic Potential-Modulated Spin Relaxation Magnetic Resonance. *Science* **1998**, *279*, 1925–1929.

(38) Atkins, P. W. Relaxation Studies III. Electron spin relaxation by phonon modulation of the hyperfine interaction tensor. *Mol. Phys.* **1967**, *12*, 201–209.

(39) Abalmassov, V. A.; Marquardt, F. Electron-nuclei spin relaxation through phonon-assisted hyperfine interaction in a quantum dot. *Phys. Rev. B* **2004**, *70*, 075313.

(40) Independent optical spectroscopic measurements also suggest the presence of an unidentified impurity in the depleted Zn metal precursor.

(41) Madelung, O. *Semiconductors: Data Handbook*, 3rd ed.; Springer: Berlin, 2004.

(42) Pandey, A.; Guyot-Sionnest, P. Slow Electron Cooling in Colloidal Quantum Dots. *Science* **2008**, *322*, 929–932.

(43) Tyryshkin, A. M.; Lyon, S. A.; Astashkin, A. V.; Raitsimring, A. M. Electron spin relaxation times of phosphorous donors in silicon. *Phys. Rev. B* **2003**, *68*, 193207.

(44) Merkulov, I. A.; Efros, A. L.; Rosen, M. Electron Spin Relaxation by Nuclei in Semicondutor Quantum Dots. *Phys. Rev. B* **2002**, *65*, 205309.

(45) Goodman, B. A.; Raynor, J. B. Electron Spin Resonance of Transition Metal Complexes. In *Advances in Inorganic Chemistry and Radiochemistry*; Emeléus, H. J., Sharpe, A. G., Eds.; Academic Press: New York, 1970; Vol. 13, pp 135−362.

(46) Morton, J. R.; Preston, K. F. Atomic parameters for paramagnetic resonance data. *J. Magn. Reson.* **1978**, *30*, 577–582.

(47) Badaeva, E.; Feng, Y.; Gamelin, D. R.; Li, X. Investigation of Pure and Co^{2+}-Doped ZnO Quantum Dot Electronic Structures using Density Functional Theory: Choosing the Right Functional. *New J. Phys.* **2008**, *10*, 055013.

(48) Balasubramanian, G.; Neumann, P.; Twitchen, D.; Markham, M.; Kolesov, R.; Mizuochi, N.; Isoya, J.; Achard, J.; Beck, J.; Tissler, J.; Jacques, V.; Hemmer, P. R.; Jelezko, F.; Wrachtrup, J. Ultralong spin coherence time in isotopically engineered diamond. *Nat. Mater.* **2009**, *8*, 383–387.

(49) Gali, A.; Janzén, E.; Deák, P.; Kresse, G.; Kaxiras, E. Theory of Spin-Conserving Excitation of N - V^- Center in Diamond. *Phys. Rev. Lett.* **2009**, *103*, 186404.

(50) Cullis, P. R.; Marko, J. R. Determination of the Donor Pair Exchange Energy in Phosphorous-Doped Silicon. *Phys. Rev. B* **1970**, *1*, 632–637.

(51) Gordon, J. P.; Bowers, K. D. Microwave Spin Echoes From Donor Electrons in Silicon. *Phys. Rev. Lett.* **1958**, *1*, 368–370.

JP106356Y